Results in Chemistry 4 (2022) 100451

Contents lists available at ScienceDirect

Results in Chemistry

journal homepage: www.sciencedirect.com/journal/results-in-chemistry

Stable and magnetically separable nanocomposite prepared from bauxite mining tailing waste as catalyst in wet peroxidation of tetracycline

Elsa Dwi Ana Santosa [a], Muchammad Tamyiz [b,c], Suresh Sagadevan [d], Arif Hidayat [e], Is Fatimah [a,*], Ruey-an Doong [b]

[a] Department of Chemistry, Faculty of Mathematics and Natural Sciences, Universitas Islam Indonesia, Kampus Terpadu UII, Jl. Kaliurang Km 14, Sleman, Yogyakarta 55584, Indonesia
[b] Universitas Nahdlatul Ulama Sidoarjo, Jl. Monginsidi Kav DPR No. Dalam, Sidoklumpuk, Sidokumpul, Kec. Sidoarjo, Kabupaten Sidoarjo, Jawa Timur 61218, Indonesia
[c] Institute of Analytical and Environmental Sciences, National Tsing Hua University, 101, Sec 2, Kuang Fu Road, Hsinchu 30013, Taiwan
[d] Nanotechnology & Catalysis Research Centre, University of Malaya, Kuala Lumpur 50603, Malaysia
[e] Department of Chemical Engineering, Faculty of Industrial Technology, Universitas Islam Indonesia, Kampus Terpadu UII, Jl. Kaliurang Km 14, Sleman, Yogyakarta 55584, Indonesia

ARTICLE INFO

Keywords:
Advanced oxidation process
Catalytic wet peroxidation
Magnetic
Nanocomposite
Mining waste

ABSTRACT

The purpose of this study is to convert bauxite mining tailing waste into magnetic nanocomposite as catalyst in catalytic wet peroxidation of tetracycline. The preparation of material was performed via hydrothermal method of immobilized iron oxide precursor of Fe^{2+} and Fe^{3+} in alkaline condition, followed by calcination. The obtained nanocomposite was characterized using X-ray diffraction, scanning electron microscopy-energy dispersive X-ray spectroscopy, transmission electron microscopy, X-ray photoelectron spectroscopy, and vibration sample magnetometer. The results from XRD, XPS and TEM analyses showed that the composite composed as the dispersed γ-Fe_2O_3 in combination with Fe_3O_4 nanoparticles. The catalytic activity studies of the nanocomposite showed the capability of material to remove tetracycline with supportive adsorption capability. The oxidation of tetracycline was recorded to follow pseudo-first kinetics with removal efficiency of 89.7 % for 20 ppm of tetracycline. Insignificant change of removal efficiency at varied tetracycline concentration ranging at 2–40 ppm indicated its potential to be active in wide range of concentration. In addition, the nanocomposite showed stability as studied by XRD analysis along with the easy in separation as the magnetic properties with magnetism of 9.8 emu/g.

1. Introduction

Management and processing of mining waste are very important for the sustainability of the mining industry itself. One of mining industries is bauxite mining, which produces huge soil residue as mining tailing waste [32]. In Indonesia, bauxite mining tailings waste (BTW) is quite large because Indonesia is one of the world's producers of bauxite with a production capacity of more than 300,000 tons per year. The concept of recycling mine waste is one strategy to minimize the environmental impact of tailings waste [4]. Several BTW from several mining industries have kaolinitic materials characteristics, and can be explored into functional materials [16,24]. Modifications of tailings waste material into functional materials to support environmental applications are mostly related to adsorption, photocatalysis and catalysis as well as geopolymerization to form brick composites or building paving materials [3,12,26,28]. Conversion of mining tailing waste as the catalyst for sustainable environment is one of the interesting topics. With the aluminum and clay-mineral contents in the BTW, the solid modification into catalyst with a functional property can be a potential strategy to support mining industry itself. Magnetic nanocomposites (MNC) are reported as good candidates for the development of high capacity adsorbents, catalyst, and photocatalysts [1,18,21]. With saturation magnetization, magnetic iron oxide-based nanocomposites provide a cost-effective approach in adsorption and photocatalysts by their ease of recovery and reuse [19,33]. Improvements in material performance related to selectivity or affinity for the specific contaminants can be

* Corresponding author.
E-mail address: isfatimah@uii.ac.id (I. Fatimah).

https://doi.org/10.1016/j.rechem.2022.100451
Received 26 May 2022; Accepted 21 July 2022
Available online 25 July 2022

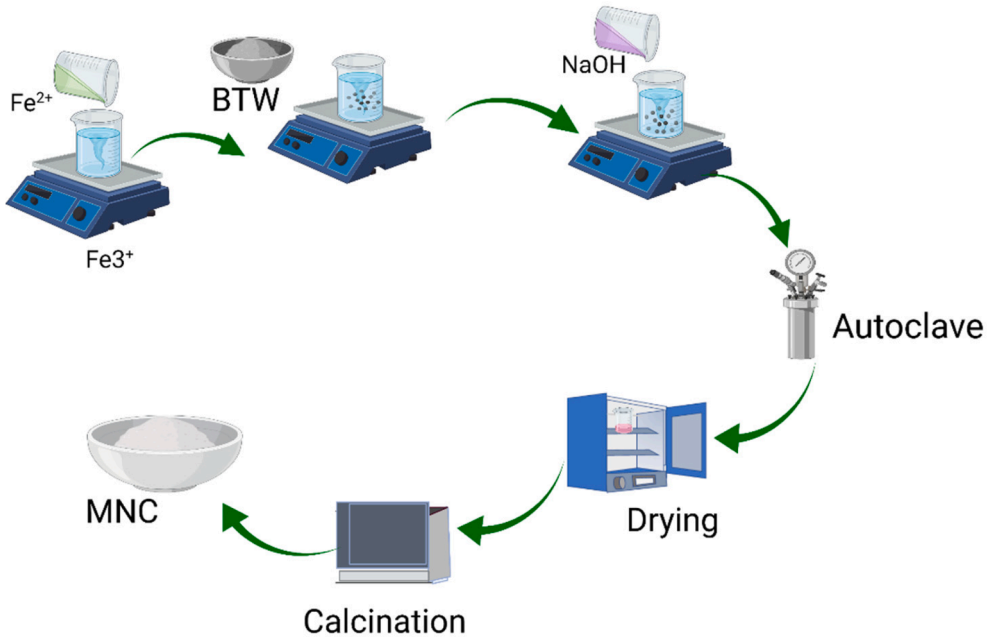

Fig. 1. Schematic representation of MNC synthesis from BTW.

accomplished by surface modification and in combination with solid support features [31]. The high adsorption capacity of the BTW is matched by the high surface area emanating from the clay structure, and the net negative charge on the structure, which attracts and retains cations such as heavy metals and cationic molecules. Moreover, the increasing attention to the use of MNC, especially magnetic iron oxide nanocomposites can be seen from the popularity based on the recent publications [20,31].

On the other hand, wastewater pharmaceutical industry is still a serious problem that is faced with regards to toxicity and the need for high-security treatment. The characteristics of pharmaceutical industry waste, such as high levels of organic pollutants, persistent and stable compounds and life-threatening toxicity, require technology that ensures the quality of processed products that are safe for the environment. In its development, the Advanced Oxidation Process (AOPs) with magnetic nanocomposite catalysts provides its own advantages. Based on these backgrounds, converting BTW to be MNC is a novel innovation as an alternative for handling mining waste, and in same time, it contributes for strengthening the applicability of the waste to be functional material for other environmental problem, particularly in AOPs. this research synthesized MNC from BTW, studied the physicochemical characteristics, and the examination on its use as catalyst for TC under AOPs. Physicochemical character of the material was carried out using instrumental analyzes such as scanning electron microscopy-energy dispersive X-ray (SEM-EDS), X-ray photoelectron spectroscopy (XPS), X-ray diffraction (XRD), transmission electron microscopy (TEM) and vibration sample magnetometer. The catalytic activity performance of MNC was based on the AOPs kinetics parameters.

2. Materials and method

2.1. Materials

BTW was collected from the Bauxite mining industry, Belitong, Indonesia. The material was prepared by drying at oven for 2 h followed crushing in a mortar to obtain a 100-mesh powder. Chemicals consist of $FeSO_4{\cdot}7H_2O$, $FeCl_3{\cdot}6H_2O$, NaOH, tetracycline hydrochloride (TC), and H_2O_2 were in pro analyst grade purchased from Merck-Millipore (Germany).

2.2. Preparation of MNC

MNC was prepared by mixing the BTW powder with iron oxide precursor, in which the iron oxide precursor was prepared by mixing $FeSO_4{\cdot}7H_2O$ with $FeCl_3{\cdot}6H_2O$ under the Fe^{3+}:Fe^{2+} molar ratio of 2:1 in double distilled water. Into the mixture, 1.0 M of NaOH solution was added slowly, until the pH of the mixture reached 8. The mixture was hydrothermally treated in a Teflon-lined autoclave at 150 °C for overnight. The suspension obtained from these steps was then dried in oven before was calcined at 400 °C in a muffle furnace. The schematic representation of MNC preparation is presented in Fig. 1.

2.3. Characterization of materials

Physicochemical characteristics of MNC in comparison with BTW were studied by XRD, SEM-EDS, TEM, and VSM analyses. X-ray diffraction (XRD) analysis was performed on a Shimadzu XRD X6000 instrument (Tokyo, Japan). A Ni-filtered Cu-Kα radiation (λ = 0.154060 nm) was used to perform the analysis for recording at the range of 2-70°. For surface morphology and elemental analysis studies, SEM-EDS (Phenom-X; Philadelphia, US) were employed, meanwhile TEM images were taken on JEOL instrument, meanwhile X-ray photoelectron spectroscopy (XPS) was performed on V.G. Scientific ESKALAB MKI microscope (Tokyo, Japan). TEM was operated at the applied voltage of 200 kV, and a monochromatic Al K_α radiation with a photon energy of 1486.6 ± 0.2 eV. The sample was degassed at the pressure below 10^{-8}Pa for 4 h before analysis. Magnetism of the materials was recorded on vibration sample magnetometer (VSM)-BHV-5 (Tokyo, Japan).

2.4. Catalytic activity study

The catalytic activity of MNC was evaluated in AOPs of TC using a batch catalytic reactor (Reflux system). Particularly, about 1 g/L of MNC powder was added into the mixture of TC solution and H_2O_2 solution (0.5 mM). The mixture was heated until Reflux point reached, and the sampling from the reaction was conducted at certain time. The TC concentration was determined by the spectrophotometric method using a U-2010 UV–visible spectrophotometer (Hitachi, Singapore). The removal efficiency of the reaction was calculated using the following Eq. (1):

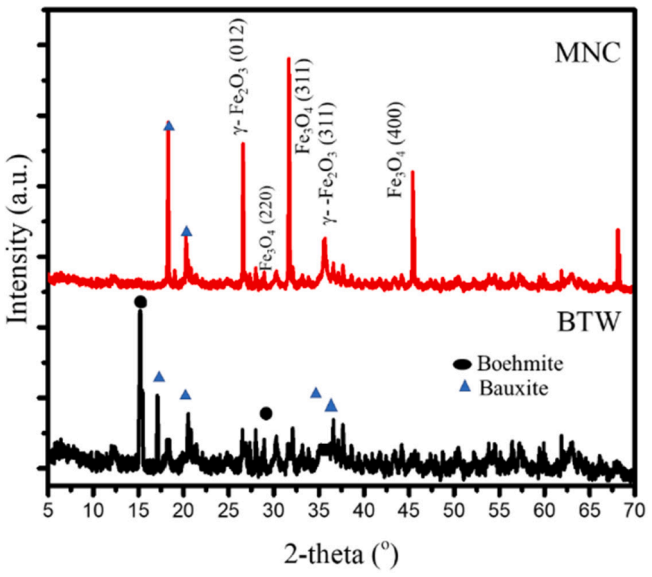

Fig. 2. XRD patterns of BTW and MNC.

Table 1
Crystallite size of γ-Fe_2O_3 and Fe_3O_4 in MNC.

		FWHM (unit)	Crystallite size (nm)	Mean
γ-Fe_2O_3	(012)	0.123	75.5	
	(220)	0.136	67.1	69.3
	(220)	0.135	65.4	
Fe_3O_4	(311)	0.136	67.1	
	(400)	0.102	94.1	80.6

$$Removal\ efficiency(\%) = \frac{C_0 - C_t}{C_0} \times 100 \quad (1)$$

With C_o and C_t are the initial concentration and concentration at sampling time t of TC.

In order to make sure that the degradation occurred during the reaction, high performance liquid chromatography (HPLC) analysis was performed on Waters (Singapore). The analyses were performed using citric acid and methanol (1:1) as used as the mobile phase on a flow rate of 1.2 mL/min.

3. Results and discussion

3.1. Physicochemical character of materials

Fig. 2 shows the reflection of BTW and MNC samples from XRD analysis.

The BTW sample show some reflections associated with the presence of boehmite and bauxite as the characteristic of the rest minerals of bauxite mining waste [25]. After was converted into MNC, some of these peaks are still maintained, mainly from the bauxite mineral, and in addition, the supported iron oxides are identified from two phases of iron oxides consist of γ-Fe_2O_3 and Fe_3O_4. The presence of γ-Fe_2O_3 is recorded by the peaks attributed to (220), (012), and (311) refer to the standard data JCPDS no. 4–755 [18,27,29,30]. Meanwhile, Fe_3O_4 is attributed to the reflections associated with (311) and (400) refer to JCPDS No. 79–0417 [11,35]. By using the Scherer formula for the identified planes, the particle size of γ-Fe_2O_3 and Fe_3O_4 were estimated. The formula is as follow (eq.2):

$$d = k\lambda / B\cos\theta \quad (2)$$

where d is the mean crystalline size of LDHs, λ is the wavelength of radiation (1.5406°A), θ is angle of selected reflection, and B is the intensity of full width at half maximum (FWHM) of the selected reflection.

Based on the calculation as listed in Table 1, the crystallite size of γ-Fe_2O_3 and Fe_3O_4 are approximately 71.3 and 61.3 nm, respectively.

The presence of both oxides is the identification of phase change during the thermal process to the iron precursor of iron chloride. Theoretically, the magnetite was formed at the temperature range of 200–300 °C, and furthermore converted into γ-Fe_2O_3 at the increasing temperature until 500 °C [9,23].

The presence of both iron oxide phases is confirmed by SEM-EDX and the TEM analysis that the figures presented in Figs. 3 and 4. The elemental analysis presented in Table 2 revealed the additional amount of iron in the MNC sample compared to BTW, as an indication of the existing oxide phase formation.

From the SEM images, it can be seen that there is no such significant change of the surface morphology which the aggregates appeared on surface. By the content of about 30 % in the composite, such more aggregates with flaky structure. It is similar with the surface feature of the magnetic nanocomposites produced using kaolinite materials [8,17].

Furthermore, the layer structures are confirmed by TEM analysis presented in Fig. 4b. In more detail, the identified lattice fringes from Fig. 4c and 4d, the lattice fringes are appeared with the interplanar distances of 0.26 and 0.36 nm that are ascribed to the (311) planes of Fe_3O_4 and (102) plane of γ-Fe_2O_3, respectively.

The presence of two phases of iron oxides is strengthened by the XPS spectra presented in Fig. 5. The survey scan in Fig. 5a represented the atoms contained in the nanocomposite are dominantly Al, Si, and Fe. The Fe existence is associated with peaks at around 700–900 eV representing the peak of Fe 2p and Fe LLM spectra. The 2p spectrum of Fe consist of 2 peaks at 709 and 722 eV, which are attributed to Fe $2p_{3/2}$ and Fe $2p_{1/2}$, respectively. The presence of Fe_3O_4 phase is assigned to the Fe LMM a–c peaks that are observed. Moreover, the deconvolution to the Fe $2p_{3/2}$ spectrum shows that the peak is composed of doublets peaks at 708.5 eV and 709.4 eV, associated to the Fe^{2+} and Fe^{3+} ionic states. From the intensity of these peaks, it is found that Fe^{2+}: Fe^{3+} peak intensity ratio showed of 0.541, which is matched with the theoretical relative composition of of $Fe^{2+}/Fe^{3+} = 0.5$ in Fe_3O_4 structure [34]. This ratio is referred to that the structure of Fe_3O_4 is composed of one Fe^{3+} on a tetrahedral site, and the other Fe^{3+} distributed on octahedral sites. The higher ratio from the peak compared to the theoretical value is also confirmed the existence of Fe_2O_3 phase as presented by XRD analysis, which is referred to the satellite peak at 716.2 eV.

Magnetic property of MNC was examined by VSM analysis with the result presented in Fig. 6.

The VSM plot can be inferred that MNC expressed superparamagnetic characteristics with the saturation magnetization value (M_s) of approximately 9.8 emu g^{-1}. This low magnetism is associated with the presence of mixed iron oxide phases of Fe_3O_4 and γ-Fe_2O_3 together with other metal oxides in BTW. However, although the magnetism is low, from the physical experiment, the catalyst can be easily attracted by magnetic field, suggesting the easy separation and collection from the reaction system by using an external magnet.

3.2. Catalytic activity of MNC

In order to test the activity of the MNC, catalytic wet peroxidation (CWPO) of TC solution with H_2O_2 as oxidant was examined using the material. Reaction was conducted at the temperature of 95 °C. Fig. 7a depicts the kinetics of TC removal by CWPO in comparison with adsorption process at room temperature (RT) and 95 °C. The kinetics plots were derived from the experiment on 20 mg/L of TC with catalyst dosage of 0.6 g/L and H_2O_2 of 3 %. The plots imply the significant role of CWPO process over the adsorption process as shown by the higher removal of TE at all varied time of treatment. The removal efficiency is 78.7 % at 120 min. However, either the adsorption at room temperature or at 95 °C exhibit the TC removal at around 45–50 %, respectively after

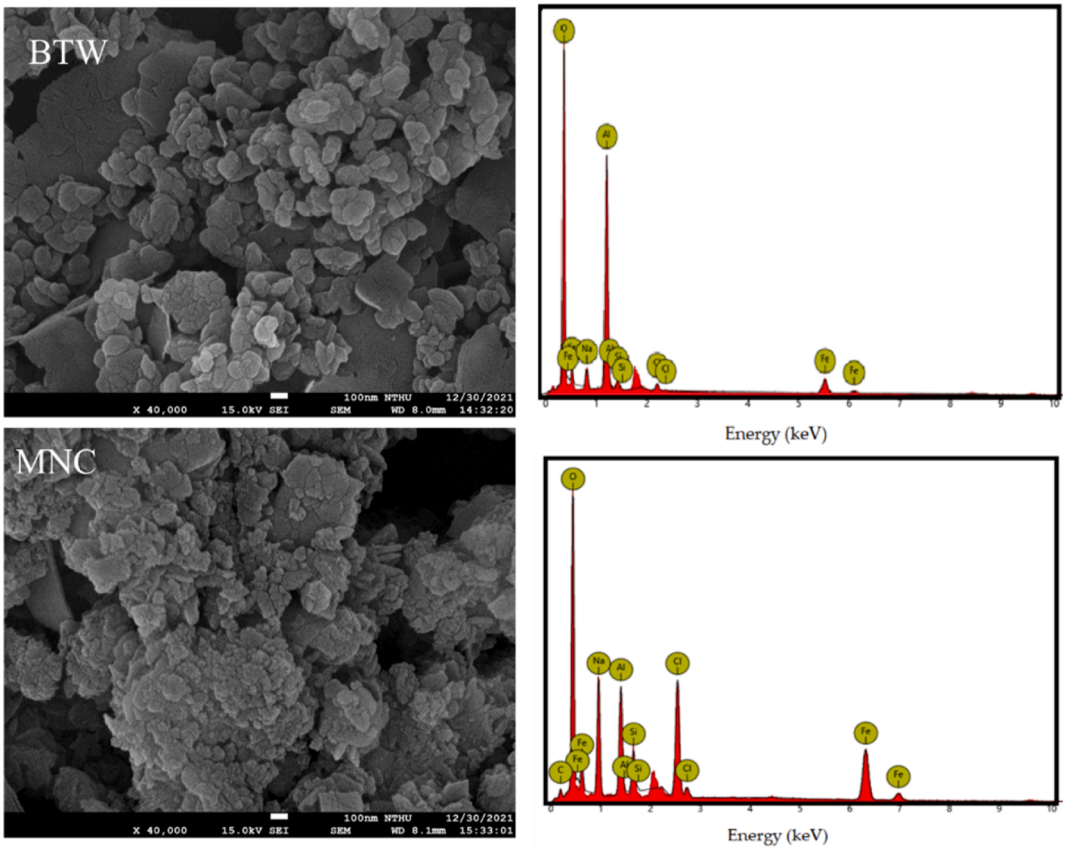

Fig. 3. SEM-EDS profiles of BTW and MNC.

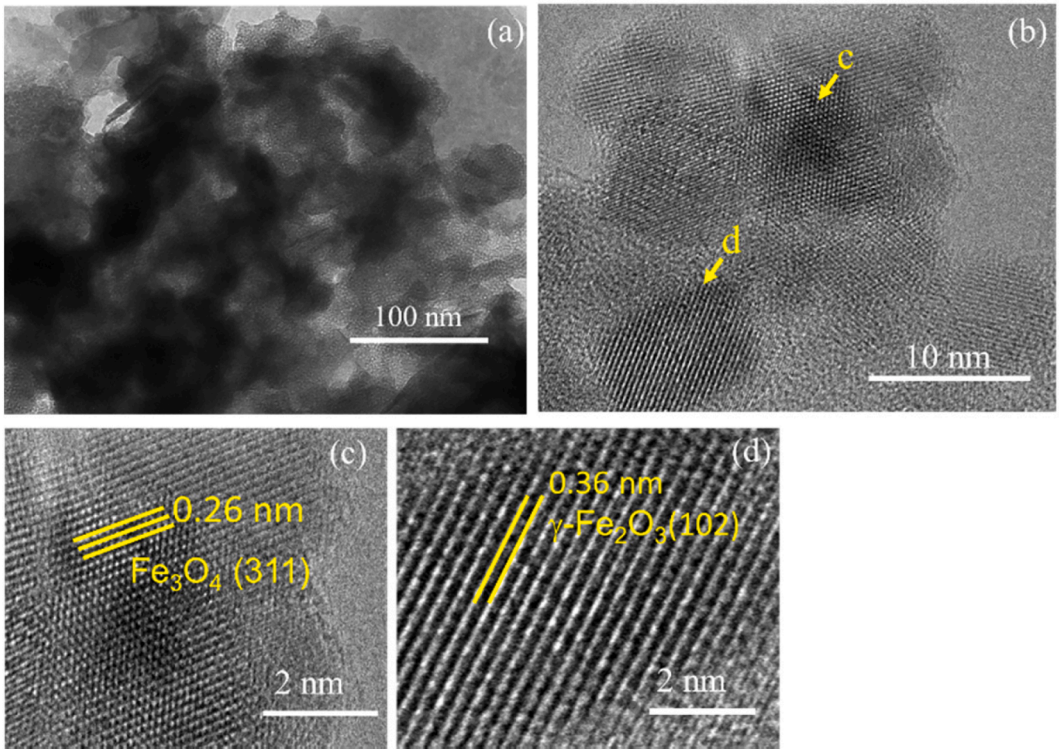

Fig. 4. TEM images of MNC in different magnifications.

Table 2
Elemental analysis of BTW and MNC from EDS analysis.

Element	BTW	MNC
O	51.30	51.47
Al	30.20	6.01
Fe	12.83	39.61
Na	2.83	5.14
Si	1.67	2.43
Cl	1.18	5.95

120 min of reaction time. This compared plots explain the presence of adsorption mechanism as important step of CWPO process. This assumption is also proven by the same removal values at 30 min of treatment, indicating time reachable for adsorption equilibrium step. In addition, the slight difference of removal at continuing time suggests that thermal treatment on adsorption is not significantly increased the kinetics of reaction. Conclusively, the CWPO process is attributed to the role of adsorption together with H_2O_2 under heating condition to decompose TC.

The high removal efficiency of the CWPO process is related to the structure of MNC which contains two phases of Fe_3O_4 and γ-Fe_2O_3. Both ionic states contribute to the radicals formation in the presence of H_2O_2 for TC oxidation via following mechanism:

$$Fe^{2+} + H_2O_2 \rightarrow Fe^{3+} + OH^- + {}^{\bullet}OH$$

$$RH + {}^{\bullet}OH \rightarrow TC^{\bullet} + H_2O$$

$$TC^{\bullet} + Fe^{3+} \rightarrow product + Fe^{2+}$$

$$Fe^{2+} + {}^{\bullet}OH \rightarrow Fe^{3+} + OH^-$$

$$Fe^{3+} + H_2O_2 \rightarrow Fe^{2+} + H^+ + HO^{\bullet}$$

Based on the mechanism, either oxidation of Fe^{2+} or reduction of Fe^{3+} play role for the TC degradation [22].

Further evaluation on TC removal was performed by calculating the kinetics of reaction. Kinetics study to the experimental data from CWPO was performed by applying pseudo-first order, pseudo-second order, and pseudo-second order kinetics following equations, respectively (eq.2–4):

$$ln\frac{C_t}{C_0} = -k_1 t \quad (2)$$

$$\frac{1}{C_t} = k_2 t + \frac{1}{C_0} \quad (3)$$

$$\frac{1}{C^2{}_t} = 2k_3 t + \frac{1}{C^2{}_0} \quad (4)$$

where C_t and C_0 are TC concentration at initial time and at time of *t*, k_1 is first-order kinetics constant, k_1, k_2, k_3 are pseudo-first, second, and third-order kinetics constants, respectively. The calculated parameters are presented in Table 3.

Refer to the R^2 values, it can be concluded that the CWPO reaction fits with pseudo-first order reaction rather than other tested kinetics order, which the pseudo-first order plot is presented in Fig. 7b. The appropriateness of the pseudo first-order model represents that the concentration of TC determines the reaction rate at the condition of catalyst dose is constant. As the proof of the occurrence of degradation instead of the reducing concentration by adsorption process, Fig. 7c shows the spectra of TC at the initial condition and treated form for an hour. There is not only a decreasing absorbance at the maximum wavelength of 359 nm, but the disappearance of the peaks at both 359 and 280 nm that are characteristics for TC. The shifting maximum wavelength is the indication of the change of molecular structure as a proof of the degradation mechanism. This is also consistence with the HPLC analysis result presented in Fig. 7d. The initial TC solution shows the intense peak associated with TC at the retention time of 7.49 min, and then after treated for 120 min, the peak is absence. The small peaks are identified at the less retention time around 1.42–2.72 min, are assigned to the presence of the molecules with lower molecular weight.

The kinetics of TC removal by adsorption process can be useful to predict the presence of chemical interaction among the catalyst and TC.

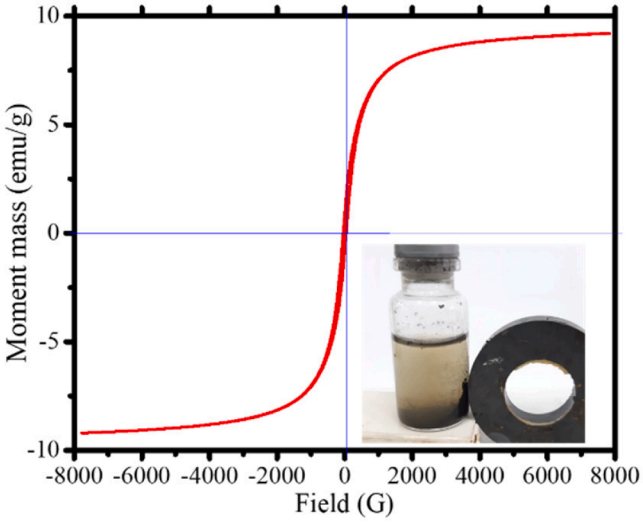

Fig. 6. VSM plot of MNC (inset: magnetic attraction experiment).

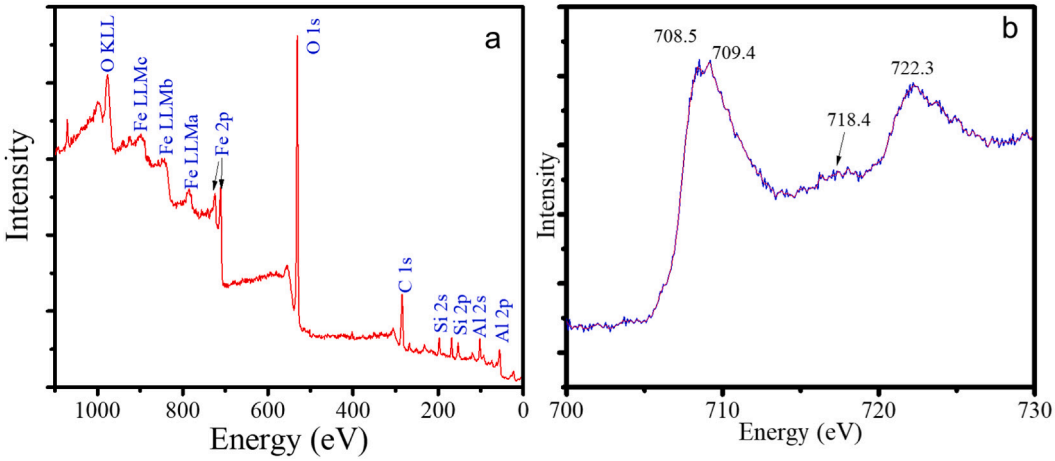

Fig. 5. a. Survey scan of MNC b. Spectrum of Fe 2p.

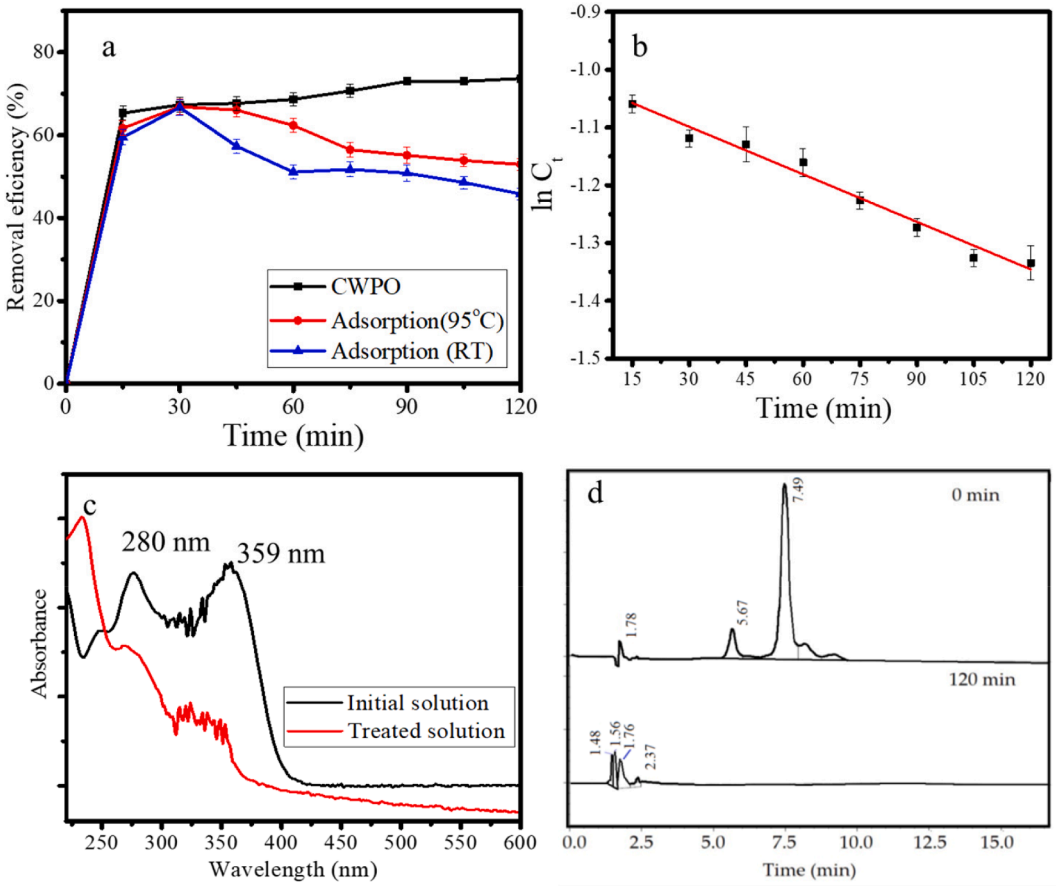

Fig. 7. a. Kinetics of TC removal over AOPs, adsorption at room temperature (RT), and at 95 °C, b. Pseudo-first order plot of TC removal by AOPs VSM plot of MNC; c. UV–vis spectra of initial TC solution and treated solution for 1 h; d. HLPC chromatogram of initial and treated solution for 120 min.

Table 3
Calculated parameters from kinetics studies.

Kinetics order	Kinetics equation	R^2
Pseudo-first order	$ln\frac{C_t}{C_0} = -2.074x10^{-3}t + 1.01$	0.989
Pseudo-second order	$\frac{1}{C_t} = 9.17x10^{-3}t + 6.62x10^{-2}$	0.978
Pseudo-third order	$\frac{1}{C^2_t} = 2.72t + 7.14$	0.984

The data was evaluated based on Lagergren's pseudo-first order, Ho and McKay's pseudo-second order, and Weber and Morris' intraparticle diffusion models with following equations (2–4).

$$\ln(q_e - q_t) = lnq_e - kt \quad (2)$$

$$\frac{t}{q_t} = \frac{1}{k_2 q_e^2} + \frac{t}{q_e} \quad (3)$$

$$q_t = k_i t^{0.5} + C \quad (4)$$

where q_t (mg/g) is the amount of adsorbed metal ions at time t, q_e (mg/g) is the adsorption capacity, k (min^{-1}) is the first-order rate constant, k_2 (g/mg min) is the second-order rate constant of adsorption (min^{-1}), and k_i ($mg.min^{1/2}/g$) and C are the kinetic constant and constant of the intra-particle diffusion model, respectively [14,37].

The calculated parameters are presented in Supplementary Information Table 1.

From the R^2 parameters, it is conclusively obtained that at both varied temperatures, the adsorption fits to the intra-particle diffusion model rather than other kinetics order. It is also seen that by k_i and C values, the adsorption equilibrium enhanced by thermal treatment. The appropriateness of this internal diffusion model implies that internal diffusion of TC by MNC is the slowest step, resulting in the rate-controlling step during the adsorption process, and the adsorption is instantaneously occurred. The higher adsorption–desorption equilibrium obtained at the increasing temperature suggest a chemisorption

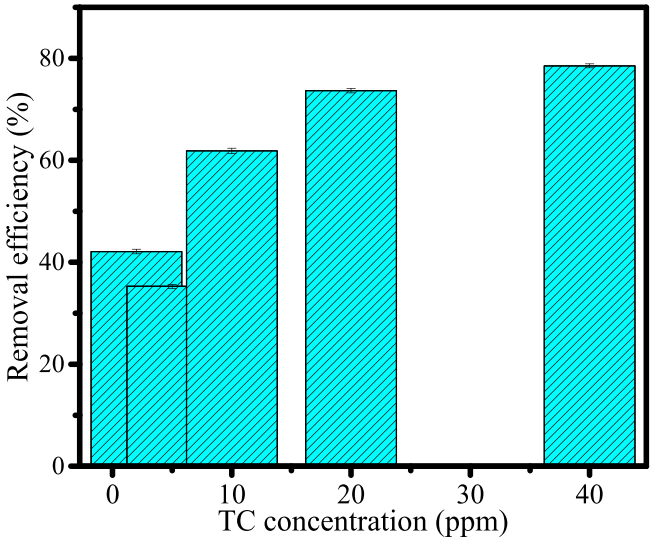

Fig. 8. Removal efficiency as function of TC concentration in CWPO.

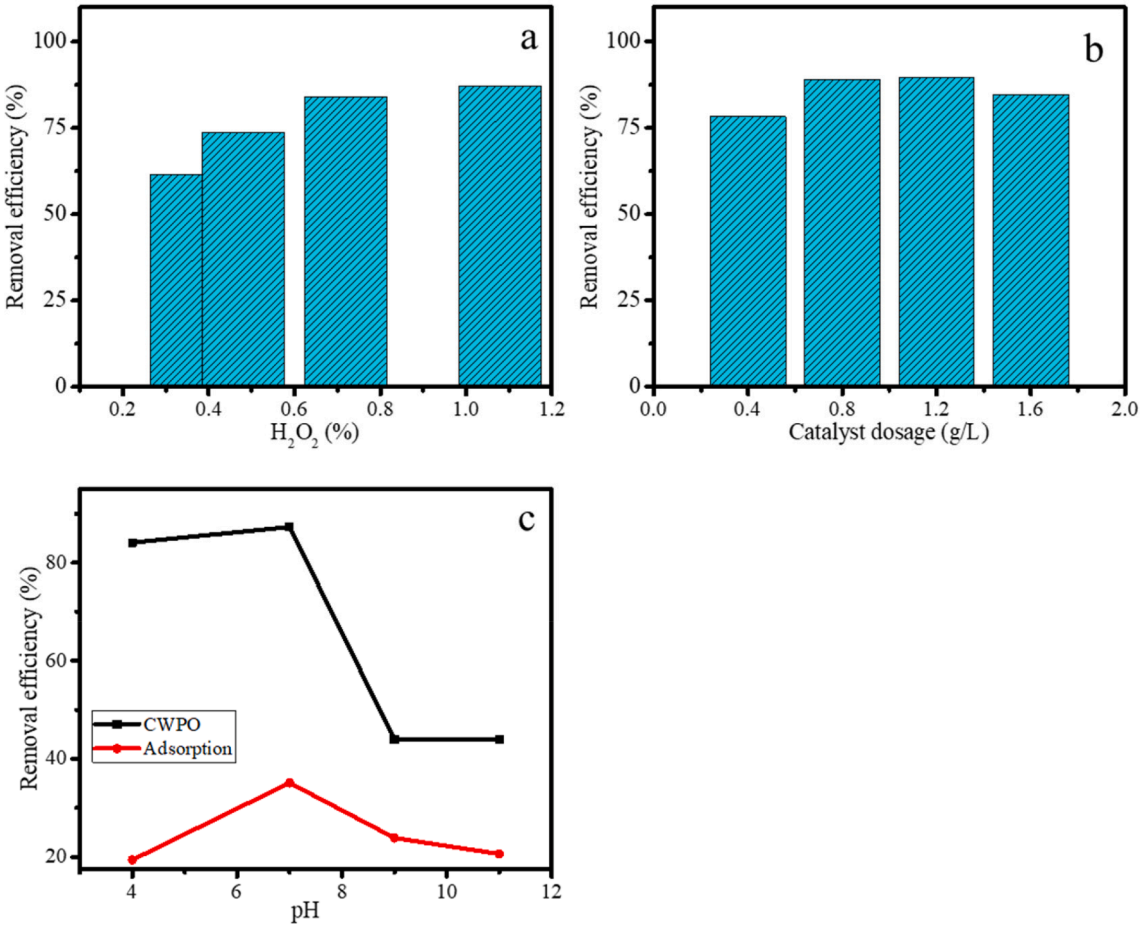

Fig. 9. Removal efficiency as function of (a) H_2O_2 concentration (b) Catalyst dosage (c) pH {TC: 20 mg/L, time of reaction: 60 min}.

mechanism rather than physisorption. Moreover, the contribution of the adsorption mechanism tends to be related with the open structure identified by surface morphology from SEM image of the MNC.

3.3. *Effect of TC concentration, catalyst dosage, H_2O_2 concentration, and pH*

The TC removal by CWPO process at varied TC concentration was examined in order to see the capability of the process at large range of concentration. The removal as function of initial TC concentration can be seen in Fig. 8.

As generally the reaction tends to be slower at the increasing reactant concentration [15], the chart in Fig. 8 represents that the removal efficiency of TC tends to increases at the range of 2–40 ppm. This means that catalyst and the catalytic process capable to conduct the oxidation reaction at the range of the concentration without limitation within the range of concentration.

Effect of catalyst dosage, H_2O_2 concentration, and pH on removal efficiency is presented by chart in Fig. 9. As can be seen from the varied H_2O_2 concentration that at the range of 0.36 – 1.08 %, the higher H_2O_2 dosage positively correlated with the removal efficiency. This is associated with the role of radical formation which depends on the presence of H_2O_2 in the solution. With the same pattern, the increased catalyst affects to enhance the removal efficiency, but it reached optimum amount at 1.2 g/L. The increased removal is correlated with the increased number of catalytic sites provided by the higher amount of catalyst [10]. In the similar range of catalyst dosage, the same effect was also reported in TC removal by Fe_3O_4 NPs and persulfate [13]. As in the CWPO the radicals are generated by the interaction of Fe^{2+} and Fe^{3+} and H_2O_2, the increased amount of catalyst mass higher than 1.2 g/L could not produce more •OH proportionally at the same amount of H_2O_2.

Moreover, the effect of pH on TC removal presented in Fig. 9c represents that pH = 7 is the optimum condition either by adsorption mechanism or CWPO. The removal over adsorption and CWPO is ineffective at basic condition due to the possible iron precipitation such as the formation of ferric hydroxy complexes which related with Fe^{2+} and Fe^{3+} at pH above 7 [13,22]. By adsorption mechanism, the TC removal at pH = 7 is higher than at pH = 4 which suggests the role of zeta potential of the catalyst that reach zero-point charge at pH = 6.8. The neutral condition optimizes the interaction of TC and the surface as the first step in the oxidation mechanism. As in the CWPO ionic state of Fe^{2+} and Fe^{3+} play important role for initiate the production of •OH, the acidic environment is more favorable [22]. By these variations, it is conclusively obtained that all parameters are the prominent variables. Within the range of tested variables, the higher H_2O_2 and catalyst dosage simultaneously increase the removal efficiency. The notably condition of pH is that the acidic environment is more appropriate to the TC degradation mechanism. It can be seen that the optimum removal efficiency can reach 89.7 % for 20 mg/L of TC under the condition of pH = 7, H_2O_2 of 5 % and catalyst dosage of 1.2 g/L.

This performance is better compared to CWPO over other catalysts such as Co_3O_4 and Fe_3O_4 nanosphere, but still less than other catalysts and in other process such as photocatalyst. The comparison with previous work on TC removal is listed in Table 4.

In summary from the comparison in Table 4, the activity of MNC catalyst in this research is less compared to other nanocomposite such as Silica supported Co_3O_4, TiO_2/Fe_3O_4/dead biomass, Fe_3O_4/g-C_3N_4, and Fe_3O_4/α-FeOOH nanocomposites that showed more than 95 % removal

Table 4
Comparison on removal efficiency in this work and other previous works.

Catalyst	Remark	Removal efficiency (%)	Reference
Fe_3O_4	Nanopartiles was applied in a CWPO using persulfate (PS). The degradation efficiency of 68.5 % was achieved on TC 0.10 mM, PS: 1.0 mM, with catalyst dose of 1 g/L for 60 min	68	[28]
$ZnFe_2O_4$/sepiolite	Removal of 78 % was achieved for 20 ppm of TC for 120 min under UV light illumination and H_2O_2 of 1 mM.	78	[29]
TiO_2/Fe_3O_4/dead biomass	Removal efficiency of 98.1 % was achieved by photocatalysis using photocatalyst composed by 2:2:1 (TiO_2/Fe_3O_4/dead biomass), catalyst dose of 10 g/L, pH 6.0, TC conc. of 10 mg/L	98.1	[6]
TiO-rGO-AC	Removal efficiency of 70 % was achieved by photocatalysis usig UV light, catalyst conc. 0.8 g/L, TC conc. 40 mg/L, reaction for 3 h.	70	[29]
Fe_3O_4/α-FeOOH Nanocomposites	Nanocomposite was applied in a photo-oxidation process to TC 10 mg/L with catalyst dose of 0.5 g/L under UV light illumination. Reaction time of 90 min.	98	[7]
Fe_3O_4/g-C_3N_4	The removal efficiency of 7 % Fe_3O_4/g-C_3N_4 at pH = 3, H_2O_2 = 5 mM, and catalyst dosage of 1.0 g/L can reach 99.8 %	99.8	[5]
Silica supported Co_3O_4	Removal of 93.4 % was achieved by ozonation using catalyst for 30 mg/L TC on 1 g/L catalyst	93.4	[27]
Fe_3O_4/activated carbon fiber	TC removal was conducted by adsorption process for 10 ppm of TC.	85	[27]
CeO_2 nanoparticles	TC removal was performed by ultrasound (US)-assisted oxidation. The removal efficiency of TC was 92.6 % in the optimum oxidation conditions TC concentration of 15 mg/L, peroxomonosulfate of 50 mM, catalyst of 0.6 g/L, US power of 70 W and pH = 6.	92.6	[2]
Magnetic nanocomposite from BTW	TC removal was performed by CWPO with H_2O_2 of 0.5 mM as oxidat. The removal efficiency of TC was 73.6 % for 20 ppm of TC and 78.2 % for 40 mg/L.	73.6 % for 20 mg/L 78.2 % for 40 mg/L	This work

at the same time using the photocatalytic system. However, the MNC exhibited higher activity compared to Fe_3O_4 nanoparticles under CWPO [13] and TiO-rGO-AC under photocatalysis procedure [36]. The activity is slightly less than the use of $ZnFe_2O_4$/sepiolite as clay-based composite, but it can be noted that H_2O_2 in this work is in less concentration (0.5 mM) meanwhile the referred work utilized 1.0 mM. The reaction condition suggests that higher removal efficiency is achievable at the optimized condition such as temperature of reaction, H_2O_2 concentration, and catalyst dose. The important thing to be noted as the beneficial aspect obtained from this work is related with the use of BTW as raw material and support with simpler method in preparation.

3.4. Catalyst stability

The examination on the catalyst stability is one of the most important study the applicability in the industrial scale. The stability of catalyst can be evaluated by the maintained structure of catalyst which was determined by using XRD analysis. The reflections are presented in Fig. 10 suggest the inappreciable change of the reflections after use catalyst. This phenomenon suggests that the properties of catalyst are unchanged without losing activity. Moreover, refer to magnetic property of material is the beneficial feature to minimize the operational cost in the real water treatment system.

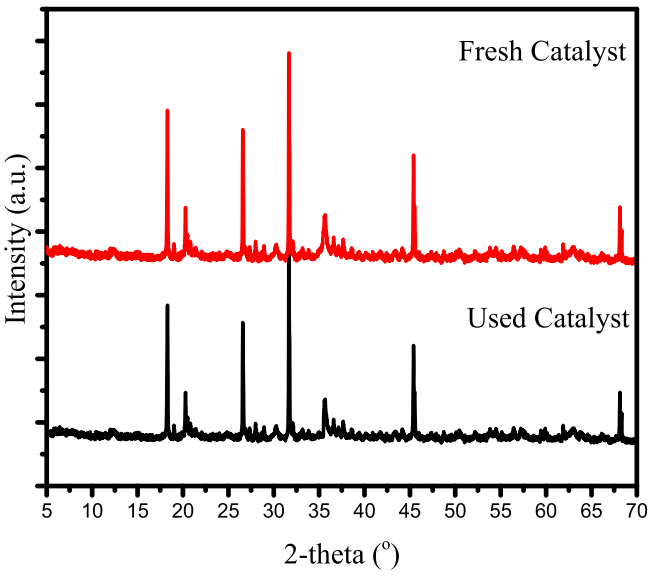

Fig. 10. XRD pattern of fresh and used catalyst.

4. Conclusion

In this study, the magnetic nanocomposite has been successfully synthesized from bauxite mining tailing waste. The nanocomposite showed the composition of immobilized γ-Fe_2O_3 and Fe_3O_4 with the crystallite size of approximately 71.3 and 61.3 nm, respectively. The nanocomposite was found to be active as catalyst in that the TC removal over advanced oxidation process using H_2O_2 as oxidant, at Reflux temperature. The removal efficiency obtained for 20 ppm of TC was 89.7 % under the catalyst dosage of 1.2 g/L and H_2O_2 of 1.0 mM for 120 min time. The results exhibited potential to be developed in mining tailing waste functionalization to support pharmaceutical wastewater treatment.

CRediT authorship contribution statement

Elsa Dwi Ana Santosa: Data curation, Software. **Muchammad Tamyiz:** Data curation. **Suresh Sagadevan:** Data curation. **Arif Hidayat:** Conceptualization. **Is Fatimah:** Conceptualization, Writing – original draft. **Ruey-an Doong:** Software, Supervision.

Declaration of Competing Interest

The authors declare the following financial interests/personal relationships which may be considered as potential competing interests: Is Fatimah reports financial support was provided by Islamic University of Indonesia. Ruey-an Doong reports a relationship with National Tsing Hua University that includes: non-financial support.

Appendix A. Supplementary data

Supplementary data to this article can be found online at https://doi.org/10.1016/j.rechem.2022.100451.

References

[1] N.H. Abdullah, K. Shameli, E.C. Abdullah, L.C. Abdullah, Solid matrices for fabrication of magnetic iron oxide nanocomposites: Synthesis, properties, and application for the adsorption of heavy metal ions and dyes, Compos. Part B Eng. 162 (2019) 538–568, https://doi.org/10.1016/j.compositesb.2018.12.075.

[2] S.N. Asadzadeh, M. Malakootian, M. Mehdipoor, D.K. Neyestanaki, The removal of tetracycline with biogenic CeO2 nanoparticles in combination with US/PMS process from aqueous solutions: Kinetics and mechanism, Water Sci. Technol. 83 (2021) 1470–1482, https://doi.org/10.2166/wst.2021.056.

[3] J. Ayala, B. Fernández, Industrial waste materials as adsorbents for the removal of As and other toxic elements from an abandoned mine spoil heap leachate: a case study in Asturias, J. Hazard. Mater. 384 (2020) 121446.

[4] J. Aznar-Sánchez, J. García-Gómez, J. Velasco-Muñoz, A. Carretero-Gómez, Mining waste and its sustainable management: Advances in worldwide research, Minerals 8 (7) (2018) 284.

[5] K.P. Cui, T.T. Yang, Y.H. Chen, R. Weerasooriya, G.H. Li, K. Zhou, X. Chen, Magnetic recyclable heterogeneous catalyst Fe3O4/g-C3N4 for tetracycline hydrochloride degradation via photo-Fenton process under visible light, Environ. Technol. (United Kingdom) (2021) 1–14, https://doi.org/10.1080/09593330.2021.1921052.

[6] G. Gopal, N. Roy, N. Chandrasekaran, A. Mukherjee, Photo-assisted removal of tetracycline using bio-nanocomposite-immobilized alginate beads, ACS Omega 4 (2019) 17487–17493, https://doi.org/10.1021/acsomega.9b02339.

[7] X. Huang, H. Zhou, X. Yue, S. Ran, J. Zhu, Novel magnetic Fe3O4/α-FeOOH nanocomposites and their enhanced mechanism for tetracycline hydrochloride removal in the visible photo-fenton process, ACS Omega 6 (2021) 9095–9103, https://doi.org/10.1021/acsomega.1c00204.

[8] I.S. Izman, M.R. Johan, R. Rusmin, Insight into structural features of magnetic kaolinite nanocomposite and its potential for methylene blue dye removal from aqueous solution, Bull. Chem. React. Eng. Catal. 17 (2022) 205–215, https://doi.org/10.9767/bcrec.17.1.12733.205-215.

[9] B. Kalska-Szostko, U. Wykowska, D. Satula, P. Nordblad, Thermal treatment of magnetite nanoparticles, Beilstein J. Nanotechnol. 6 (2015) 1385–1396, https://doi.org/10.3762/bjnano.6.143.

[10] J. Kaushik, Himanshi, V. Kumar, K.M. Tripathi, S.K. Sonkar, Sunlight-promoted photodegradation of Congo red by cadmium-sulfide decorated graphene aerogel, Chemosphere 287 (2022) 132225.

[11] I. Kazeminezhad, S. Mosivand, Phase transition of electrooxidized Fe3O4 to γ and α-Fe2O3 nanoparticles using sintering treatment, Acta Phys. Pol. A 125 (2014) 1210–1214, https://doi.org/10.12693/APhysPolA.125.1210.

[12] P. Kinnunen, A. Ismailov, S. Solismaa, H. Sreenivasan, M.L. Räisänen, E. Levänen, M. Illikainen, Recycling mine tailings in chemically bonded ceramics – A review, J. Clean. Prod. 174 (2018) 634–649, https://doi.org/10.1016/j.jclepro.2017.10.280.

[13] D. Lee, S. Kim, K. Tang, M. De Volder, Y. Hwang, Oxidative degradation of tetracycline by magnetite and persulfate: Performance, water matrix effect, and reaction mechanism, Nanomaterials 11 (9) (2021) 2292.

[14] W. Lee, S. Yoon, J.K. Choe, M. Lee, Y. Choi, Anionic surfactant modification of activated carbon for enhancing adsorption of ammonium ion from aqueous solution, Sci. Total Environ. 639 (2018) 1432–1439, https://doi.org/10.1016/j.scitotenv.2018.05.250.

[15] L. Luo, D. Zou, D. Lu, F. Yu, B. Xin, J. Ma, Study of catalytic ozonation for tetracycline hydrochloride degradation in water by silicate ore supported Xo3O4, RSC Adv. 8 (2018) 41109–41116.

[16] D. Ma, Z. Wang, M. Guo, M. Zhang, J. Liu, Feasible conversion of solid waste bauxite tailings into highly crystalline 4A zeolite with valuable application, Waste Manag. 34 (2014) 2365–2372, https://doi.org/10.1016/j.wasman.2014.07.012.

[17] A. Magdy, Y.O. Fouad, M.H. Abdel-Aziz, A.H. Konsowa, Synthesis and characterization of Fe3O4/kaolin magnetic nanocomposite and its application in wastewater treatment, J. Ind. Eng. Chem. 56 (2017) 299–311, https://doi.org/10.1016/j.jiec.2017.07.023.

[18] R. Mahajan, S. Suriyanarayanan, I.A. Nicholls, Improved solvothermal synthesis of γ-Fe2O3 magnetic nanoparticles for SiO2 coating, Nanomaterials 11 (8) (2021) 1889.

[19] M. Mishra, D.-M. Chun, α-Fe 2 O 3 as a photocatalytic material: A review, Appl. Catal. A Gen. 498 (2015) 126–141, https://doi.org/10.1016/j.apcata.2015.03.023.

[20] S. Nag, A. Ghosh, D. Das, A. Mondal, S. Mukherjee, Ni0.5Zn0.5Fe2O4/ polypyrrole nanocomposite: A novel magnetic photocatalyst for degradation of organic dyes, Synth. Met. 267 (2020), 116459, https://doi.org/10.1016/j.synthmet.2020.116459.

[21] M. Obaidullah, N.M. Bahadur, T. Furusawa, M. Sato, H. Sakuma, N. Suzuki, Microwave assisted rapid synthesis of Fe 2 O 3 @SiO 2 core-shell nanocomposite for the persistence of magnetic property at high temperature, Colloids Surfaces A Physicochem. Eng. Asp. 572 (2019) 138–146, https://doi.org/10.1016/j.colsurfa.2019.03.062.

[22] P.K. Pandis, C. Kalogirou, E. Kanellou, C. Vaitsis, M.G. Savvidou, G. Sourkouni, A. A. Zorpas, C. Argirusis, Key Points of advanced oxidation processes (AOPs) for wastewater, organic pollutants and pharmaceutical waste treatment: A mini review, ChemEngineering 6 (1) (2022) 8.

[23] V.P. Ponomar, T.S. Antonenko, O.A. Vyshnevskyi, A.B. Brik, Thermally induced changes in the magnetic properties of iron oxide nanoparticles under reducing and oxidizing conditions, Adv. Powder Technol. 31 (2020) 2587–2596, https://doi.org/10.1016/j.apt.2020.04.021.

[24] S.M.A. Qaidi, B.A. Tayeh, H.F. Isleem, A.R.G. de Azevedo, H.U. Ahmed, W. Emad, Sustainable utilization of red mud waste (bauxite residue) and slag for the production of geopolymer composites: A review, Case Stud. Constr. Mater. 16 (2022) e00994.

[25] T.R. Reddy, K. Thyagarajan, O.A. Montero, S.R.L. Reddy, T. Endo, X-ray diffraction, electron paramagnetic resonance and optical absorption study of bauxite, J. Miner. Mater. Charact. Eng. 02 (2014) 114–120, https://doi.org/10.4236/jmmce.2014.22015.

[26] M. Romero, I. Padilla, M. Contreras, A. López-delgado, Mullite-based ceramics from mining waste: A review, Minerals 11 (2021) 1–39, https://doi.org/10.3390/min11030332.

[27] S. Kakuta, T. Abe, Photocatalysis for water oxidation by Fe2O3 nanoparticles embedded in clay compound: correlation between its polymorphs and their photocatalytic activities, J. Matter. Sci. 44 (11) (2009) 2890–2898.

[28] S. Sarkar, S. Sarkar, P. Biswas, Effective utilization of iron ore slime, a mining waste as adsorbent for removal of Pb(II) and Hg(II), J. Environ. Chem. Eng. 5 (2017) 38–44, https://doi.org/10.1016/j.jece.2016.11.015.

[29] S. Sundar, G. Venkatachalam, S. Kwon, Sol-gel mediated greener synthesis of γ-Fe2O3 nanostructures for the selective and sensitive determination of uric acid and dopamine, Catalysts 8 (11) (2018) 512.

[30] Z. Tashrifi, S. Bahadorikhalili, H. Lijan, S. Ansari, H. Hamedifar, M. Mahdavi, Synthesis and characterization of γ-Fe2O3@SiO2-(CH2)3-PDTC-Pd magnetic nanoparticles: A new and highly active catalyst for the Heck/Sonogashira coupling reactions, New J. Chem. 43 (2019) 8930–8938, https://doi.org/10.1039/c9nj01562k.

[31] É. Ujaczki, V. Feigl, M. Molnár, P. Cusack, T. Curtin, R. Courtney, L. O'Donoghue, P. Davris, C. Hugi, M.WH. Evangelou, E. Balomenos, M. Lenz, Re-using bauxite residues: benefits beyond (critical raw) material recovery, J. Chem. Technol. Biotechnol. 93 (9) (2018) 2498–2510.

[32] A.S. Verma, N.M. Suri, S. Kant, Applications of bauxite residue: A mini-review, Waste Manag. Res. 35 (2017) 999–1012, https://doi.org/10.1177/0734242X17720290.

[33] J. Virkutyte, R.S. Varma, Eco-friendly magnetic iron oxide-pillared montmorillonite for advanced catalytic degradation of dichlorophenol, ACS Sustain. Chem. Eng. 2 (2014) 1545–1550, https://doi.org/10.1021/sc5002512.

[34] H. Wang, M. Zhang, H. Li, Synthesis of nanoscale zerovalent iron (nZVI) supported on biochar for chromium remediation from aqueous solution and soil, Environ. Res. Public Heal. (2019) 4430.

[35] Z. Zarnegar, J. Safari, Modified chemical coprecipitation of magnetic magnetite nanoparticles using linear-dendritic copolymers, Green Chem. Lett. Rev. 10 (2017) 235–240, https://doi.org/10.1080/17518253.2017.1358769.

[36] C. Zhang, X. Han, F. Wang, L. Wang, J. Liang, A Facile Fabrication of ZnFe2O4/Sepiolite Composite with Excellent Photocatalytic Performance on the Removal of Tetracycline Hydrochloride, Front. Chem. 9 (2021), 736369.

[37] C. Zou, J. Liang, W. Jiang, Y. Guan, Y. Zhang, Adsorption behavior of magnetic bentonite for removing Hg(II) from aqueous solutions, RSC Adv. 8 (2018) 27587–27595, https://doi.org/10.1039/c8ra05247f.